Elucidating the mechanism of cell death by bacopaside II in triple-negative breast cancer

A thesis submitted in partial fulfilment of the

HONOURS DEGREE of BACHELOR OF

HEALTH AND MEDICAL SCIENCES in

The Discipline of Physiology

Adelaide Medical School

The University of Adelaide

by Kenny Yeo Ker Li

November 2020

Abstract

Background: Triple-negative breast cancer (TNBC) is the most aggressive subtype of breast cancer. Lack of targeted therapies and chemotherapy resistance remain key issues, the latter being linked to cancer stem cells (CSCs). Previously, we showed that bacopaside II induces vacuoles and cell death in breast cancer cells, but the mechanism remains unknown. We aim to study cell death types (apoptosis, methuosis or necroptosis), and determine if bacopaside II can overcome resistance.

Methods: TNBC cell line, MDA-MB-231, was treated with bacopaside II. Caspase-3/7 activation and labelled-dextran uptake were measured to indicate apoptosis and methuosis respectively. Propidium iodide (PI) influx, with and without necrostatin-1, and immunoblot of necroptosis proteins (MLKL, phosphorylated MLKL) were measured to indicate necroptosis. Scaffold-less 3D-cultured model was established and compared to 2D-cultured cells, to measure expression of CSC markers (*OCT4*, *NANOG*), and changes in IC50 to paclitaxel, doxorubicin, 5-fluorouracil or bacopaside II to indicate resistance/sensitivity.

Results: With bacopaside II treatment, caspase-3/7 was not activated and dextran did not localize within vacuoles. Bacopaside II induced a dose-dependent increase in PI-positivity and increased pMLKL:MLKL ratio. Necrostatin-1 (50 μM) significantly reduced ($p < 0.05$) PI-positivity by 20% and 21% with 20 and 30 μM bacopaside II respectively, compared to vehicle control. 3D-cultured MDA-MB-231 displayed increases ($p < 0.0001$) in *OCT4* (3.4-fold) and *NANOG* (38-fold) expression, and increases ($p < 0.0001$) in IC50 for paclitaxel (2.1-fold), doxorubicin (2.2-fold) and 5-fluorouracil (1.4-fold) but not bacopaside II, relative to 2D-cultured cells.

Conclusion: Bacopaside II may induce necroptosis and overcomes resistance in 3D-cultured model.

1. Introduction

Triple-negative breast cancer (TNBC) is the most aggressive subtype of breast cancer, with approximately 400,000 new cases worldwide each year[1]. It is characterised by the absence of human epidermal receptor-2, progesterone and estrogen receptors, resulting in the lack of targeted treatment[2]. Women with TNBC have a poorer prognosis and higher rate of metastasis due to residual cancer burden compared to other breast cancer subtypes, despite having an initial good response to neoadjuvant chemotherapies[3]. Furthermore, chemotherapy-induced toxicity also takes a toll on the patients, affecting quality of life and treatment outcomes[4].

Due to heterogeneity, TNBC can be further categorized into subgroups based on gene-expression profile. Recently, three molecular clusters (C1-3) were defined, whereby C1 expresses luminal androgen receptor, while C2 and C3 are basal-like[5]. Additionally, C2 is immunosuppressive, while C3 expresses adaptive immune phenotype associated with immune checkpoint upregulation including PD1 and PD-L1[5]. This suggests that responses to current therapies will be different in each cluster. Furthermore, only C3 subset would respond to immunotherapy.

Cancer heterogeneity can be explained by two hypotheses: clonal evolution model and cancer stem cell (CSC) model[6]. The former postulates that all cancer cells have tumorigenic potential and sequential mutations generates heterogeneity within a tumour, while the latter proposed that only a subset of cancer cells known as CSC have tumour-propagating potential[6]. Extensive intratumor heterogeneity often leads to the development of resistance[7]. In basal-like breast cancer, CSC phenotype $CD44^{+}CD24^{-/low}$ and ALDH1 positivity were associated with higher chemoresistance, recurrence, metastasis, and poorer progression-free survival (PFS) and overall survival (OS)[8]. Moreover, TNBC patients with high OCT4 and NANOG expression have poorer PFS and OS[9, 10]. In all, the lack of targeted therapies, heterogeneity, and development of resistance in TNBC constitute the need for an alternative therapy.

Our group have been investigating bacopaside II, a purified compound from medicinal herb *Bacopa monnieri.* An extract of this herb, Brahmi, is available over the counter and has been used for centuries for memory enhancement and more recently as a sedative, with limited adverse effects reported[11-13]. Bacopaside II belongs to the family of triterpenoid saponins. Other family members exhibit anti-inflammatory effects, and anti-cancer properties including promoting apoptosis and autophagy, while inhibiting proliferation, metastasis and multidrug resistance[14]. A well-studied example, bacoside A/B, displayed anti-cancer effects in breast, colon, lung and brain cancer[15-18]. Furthermore, bacopaside II treatment have been reported to impair migration in colorectal cancer cells by blocking aquaporin-1 channels[19].

Previously, our group reported that bacopaside II induced vacuole formation in endothelial cells, breast and colorectal cancer cells by unknown mechanisms[20-22]. These findings were similar to a study from John et al.[17], whereby bacoside A (containing bacopaside II) also led to vacuole formation in glioblastoma cells, detected by tetramethylrhodamine-dextran (TMR-dextran) uptake and immunostaining of endosomal trafficking and lysosomal membrane proteins (Rab7, LAMP1), suggesting methuosis[17]. Methuosis is characterized by excessive macropinocytosis and disruption of macropinosome trafficking, leading to accumulation of large cytoplasmic vacuoles which ruptures the cell membrane[23-25]. Hence, methuosis will be investigated as a possible mechanism of cell death induced by bacopaside II.

Furthermore, we also reported significant increase in annexin-V-positive/propidium iodide (PI)-negative and annexin-V-positive/PI-positive populations in breast cancer and colorectal cancer cells, when treated with bacopaside II alone or in combination with bacopaside I[20, 21]. It was suggested that apoptosis was the mechanism of cell death[20, 21]. However, annexin-V and PI positivity are not conclusive hallmarks of apoptosis[26]. Necroptosis, a programmed necrosis pathway, can also result in annexin-V-positivity or PI-positivity, and vacuole formation[24, 27, 28].

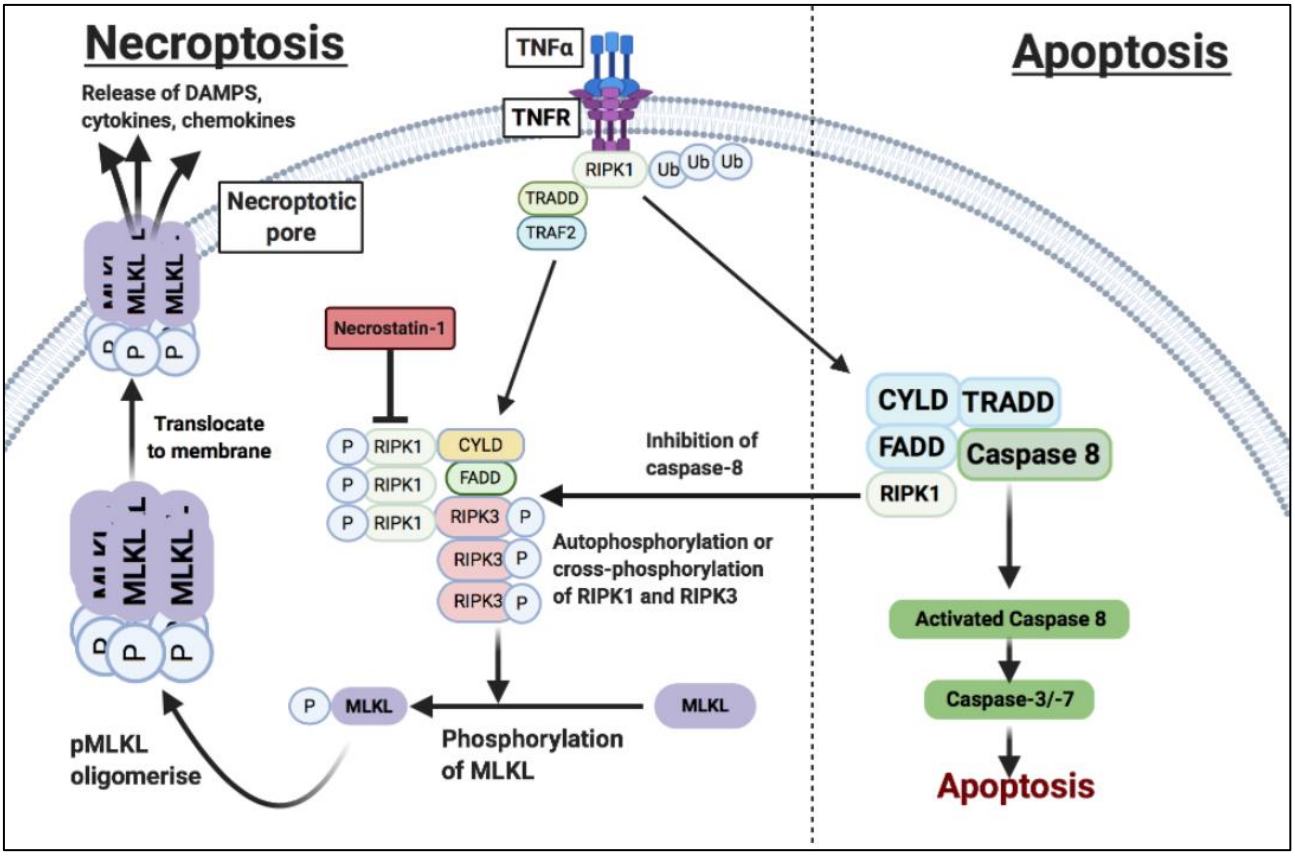

Figure 1: Interplay between necroptosis and apoptosis.

Necroptosis can be activated by ligand binding to tumour necrosis factor (TNF) family death domain receptors, which leads to activation of receptor-interacting serine-threonine protein kinase 1 and 3 (RIPK1/3), and executor mixed-lineage kinase domain-like (MLKL) protein by phosphorylation (p) (Figure 1)[29-31]. Subsequently, pMLKL oligomerizes and translocates to cell membrane to form pores, which results in ion (Ca^{2+}, Na^{+}, Mg^{2+}) influx, cell rupture and the release of damage-associated molecular patterns (DAMPs)[29-33]. With a compromised cell membrane, PI and annexin-V will be able to bind to nucleic acids and membrane phosphatidylserine respectively. Hence, markers of apoptosis (caspase-3/-7)[34] and necroptosis (MLKL, pMLKL) will be further investigated following bacopaside II treatment.

Bacopaside II also reduced cell growth, migration and survival in endothelial cells, breast and colorectal cancer cells[19-22]. Since the maintenance of normal cell growth, migration and survival is

regulated by PI3K-Akt-mTOR signalling pathway, bacopaside II may affect this pathway[35]. Furthermore, apoptosis, methuosis and necroptosis were found to be regulated by PI3K-Akt-mTOR signalling pathway, making this a relevant pathway to investigate the effects of bacopaside II[36-38].

The goal for this project is to elucidate the mechanism of cell death of bacopaside II by investigating the markers of apoptosis, methuosis and necroptosis, and transcriptomic changes in PI3K-Akt-mTOR signalling pathway. Apoptosis is a common mechanism of cell death caused by chemotherapies[39]. However, signalling pathways regulating apoptosis are often dysregulated, leading to the development, progression and resistance of the cancer[39]. Non-apoptotic cell death pathways, such as necroptosis or methuosis, may be able to bypass apoptosis resistance and benefit cancer patients. Particularly for necroptosis, the release of DAMPs initiates immunogenic responses whereby tumours can be rendered sensitive or be re-sensitised to immunotherapy regimens[29].

Here, we hypothesize that bacopaside II causes cell death through a non-apoptotic pathway, necroptosis or methuosis, which can overcome the resistance induced in a 3D-cultured cell model. The effects of bacopaside II are also postulated to influence PI3K-AKT-mTOR signalling pathway.

1.1 AIMS:

i) Elucidate the type of cell death caused by bacopaside II through analysis of molecular markers of apoptosis, methuosis and necroptosis.

ii) Determine the change in transcript expression within PI3K-AKT-mTOR signalling pathway with bacopaside II, using quantitative PCR (qPCR) on TaqMan® human PI3K signalling arrays.

iii) Develop resistance in MDA-MB-231 by culturing in 3D-culture and test the efficacy of chemotherapies (paclitaxel, doxorubicin, 5-fluorouracil) and bacopaside II on these chemo-resistant cells.

2. Materials and Methods

2.1 Drug preparation

The analytical standard bacopaside II (≥ 95% purity by HPLC) was obtained from Sigma-Aldrich (St Louis, MO, USA), and dissolved in methanol. Paclitaxel and 5-fluorouracil were purchased from Sigma-Aldrich, dissolved in dimethyl sulfoxide (DMSO; Sigma-Aldrich). Doxorubicin hydrochloride (Pfizer Australia Pty Ltd, Sydney, NSW, Australia) was obtained from The Queen Elizabeth Hospital, Adelaide.

2.2 Cell line and cell culture

TNBC cell line, MDA-MB-231, was obtained from American Type Culture Collection (ATCC, Manassas, VA, USA) and maintained in Leibovitz's L-15 Medium (Life Technologies, Eugene, OR, USA), supplemented with 10% heat-inactivated foetal bovine serum (Corning, NY, USA), 200 U/mL of penicillin and 200 µg/mL of streptomycin (Life Technologies), at 37 °C and 0% CO_2 in air. Cells were mycoplasma-free (MycoAlert^{TM} Mycoplasma detection kit; Lonza, Mt Waverley, VIC, Australia).

2.3 Apoptosis assay

To determine if cell death occurred through apoptosis, caspase-3/-7 (CellEvent™ caspase-3/7; ThermoFisher Scientific, Waltham, MA, USA) activation was measured using fluorescence channel of IncucyteS3 live-cell imaging system (Essen Bioscience, Ann Arbor, MI, USA) at 24 h. Cells were seeded at 3.3×10^3 cells per well in a 96-well flat bottom plate (Corning) and treated with various doses of bacopaside II (Table 1), with 0.25 µM staurosporine (Sigma-Aldrich) as positive control. Results were analysed by Prism v8.4.3 (GraphPad software, CA, USA), using one-way analysis of variance (ANOVA) with Dunnett's multiple comparison and presented as average caspase-3/-7 counts per image with mean ± standard error mean (SEM) (n = 6 per dose).

Table 1: Treatment doses

Drug	Doses	Vehicle
Paclitaxel (nM)	0.39, 0.78, 1.56, 3.13, 6.25, 12.5, 25, 50, 100	0.01% DMSO
Doxorubicin (µM)	0.098, 0.20, 0.39, 0.78, 1.56, 3.13, 6.25, 25, 100	Media
5-flurouracil (µM)	0.78, 1.56, 3.13, 6.25, 12.5, 25, 50, 100, 200	0.13% DMSO
Bacopaside II (µM)	2.5, 5, 10, 15, 20, 30	2% methanol

2.4 Dextran-uptake assay

To investigate if bacopaside II induced macropinocytosis, 75-kDa TMR-dextran (Sigma-Aldrich) uptake was measured to indicate macropinosomes[40]. Cells were seeded at 1×10^5 cells per well in a 8-well chamber slides (ThermoFisher Scientific), treated with 15 µM bacopaside II for 6 h, and 1 h of incubation with 1 mg/ml TMR-dextran[40]. Cells were washed with Dulbecco's phosphate buffered saline (DPBS; ThermoFisher Scientific), fixed with 4% paraformaldehyde (Sigma-Aldrich), and stained with 4′,6-diamidino-2-phenylindole (DAPI; ThermoFisher Scientific) nuclear stain. Representative images from three experiments were captured using Zeiss Axio observer Z1 inverted microscope (Carl Zeiss, Jena, Germany).

2.5 Effects of bacopaside II on cell membrane integrity

Cells were seeded at 3.3×10^3 cells per well in a 96-well plate and treated with bacopaside II as per Table 1 (n = 6, per dose). Propidium iodide (Sigma-Aldrich) was used at 2.5 µg/mL to indicate disrupted membrane integrity. Live-cell imaging was performed at 2 h intervals for two days using IncucyteS3, with phase contrast and red fluorescence images being captured. Data were analysed

using Prism v8.4.3 and presented as average PI counts per image with 95% confidence interval (CI) across two days. Two-way ANOVA with Dunnett's multiple comparison was performed to determine significant changes at each timepoints compared to vehicle control.

Further investigation included necroptosis inhibitor, necrostatin-1, to inhibit PI-influx. Cells were treated with 20 or 30 μM bacopaside II, along with 10, 20, 30, 40 and 50 μM necrostatin-1 for each bacopaside II treatment. Vehicle control contained only bacopaside II, and each condition contained 2.5 μg/mL PI. Results were analysed relative to vehicle control, using one-way ANOVA test with Dunnett's multiple comparison and presented as average PI counts per image with mean ± SEM (n = 6) at 12 h.

2.6 Western immunoblot for MLKL and pMLKL after bacopaside II treatment

MDA-MB-231 (5×10^5) were seeded into wells of a 6-well plate (Corning) and incubated overnight. Next, the cells were treated with bacopaside II for 4 h, lysed using RIPA Lysis and Extraction Buffer supplemented with Halt Protease Inhibitor Cocktail and Halt Phosphatase Inhibitor Cocktail (Thermo Fisher Scientific), homogenised by passing through a 26-gauge needle, and centrifuged at 17,000 x g for 15 min at 4 °C to remove insoluble cell debris. Total protein was quantified using Bio-Rad Protein Assay (Bio-Rad, Hercules, CA, USA) and 50 μg was resolved by denaturing electrophoresis using 4-15% Mini-PROTEAN TGX Stain-Free precast gels and transferred to 0.2 μm polyvinylidene difluoride membranes using a Trans-Blot Turbo Transfer System (Bio-Rad). Membranes were blocked with either 5% skim milk (for MLKL) or 5% BSA (for pS358-MLKL) in Tris-buffered saline supplemented with 0.05% (v/v) Tween-20 (TBST) for at least 1 h. Membranes were incubated at 4°C overnight with 1:1000 dilution anti-MLKL (clone [EPR17514], ab184718) in 0.1% milk in TBST, or 1:1000 anti-pS358-MLKL ([EPR9514], ab187091) in 2% BSA in TBST. Finally, membranes were washed 5 times with TBST, incubated with 1:2000 goat anti-rabbit (H+L)-HRP conjugated secondary antibody (Bio-Rad) for 1 h and visualised using Clarity Western ECL Blotting Substrate with a

ChemiDoc Gel Imaging System (Bio-Rad). The MLKL and pMLKL bands were quantified and normalised to total protein using Image Lab Software v6.0.1 (Bio-Rad).

2.7 3D-culture to establish resistant cell model

To establish a resistant model, three biological replicates of MDA-MB-231 were cultured in 3D scaffold-less conditions for four weeks to enhance for stem cell-like phenotypes[41]. Briefly, cells were seeded at 4 × 10^4 cells per well in ultra-low attachment (ULA) 6-well plates (Corning) using Mammocult™ media (STEMCELL™ Technologies, Vancouver, Canada), supplemented with 10% MammoCult™ proliferation supplement, 4 µg/mL heparin solution, 0.48 µg/mL hydrocortisone stock solution, 200 U/mL of penicillin and 200 µg/mL of streptomycin (Life Technologies). Mammospheres were passaged weekly by dissociating with 2% ethylenediaminetetraacetic acid (Sigma-Aldrich) in PBS and reseeding at 4 × 10^4 cells per well[41]. Mammospheres were dissociated and reseeded for subsequent experiments (Figure 2). Herein, these cells are termed 3D-cultured cells.

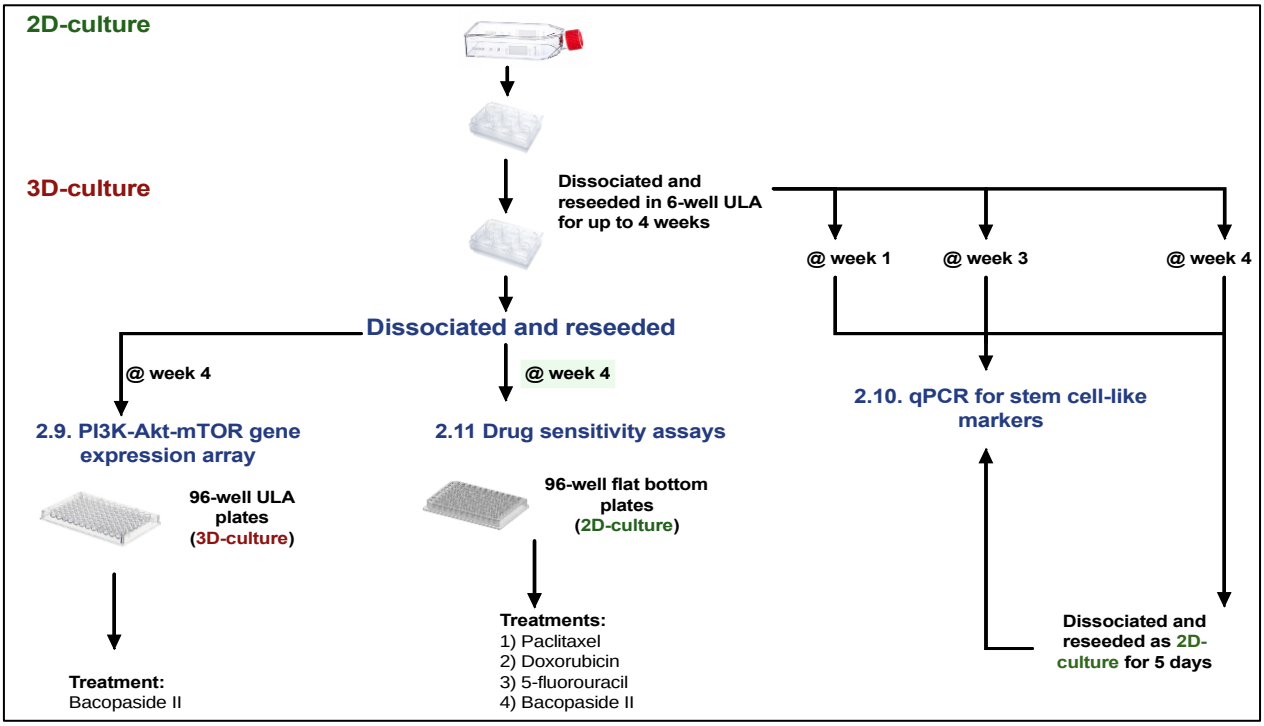

Figure 2: Experiments using 3D-cultured cells.

2.8 RNA extraction and cDNA synthesis

RNA was isolated for TaqMan® array human PI3K signalling 96-well plates and TaqMan® gene expression assays (see below) using PureLink RNA Mini Kit (Life Technologies) according to manufacturer's instructions. RNA was quantified using NanoDrop™ 2000 spectrophotometer (ThermoFisher Scientific). Total RNA (1.5 µg for TaqMan® array human PI3K signalling and 150 ng for TaqMan® gene expression assays) was reverse transcribed using SuperScript™ IV VILO Master Mix (ThermoFisher Scientific) following manufacturer's instruction.

2.9 PI3K-Akt-mTOR gene expression array

Transcript expression within human PI3K signalling pathway were studied using TaqMan® array human PI3K signalling 96-well plate (Applied Biosciences™, Foster City, CA, USA), containing 92 genes involved in PI3K signalling pathway. 3D-cultured cells were seeded at 5×10^3 cells per well in 96-well ULA plates (Corning) and treated with 15 µM bacopaside II or vehicle control (2% methanol) for 24 h. Master mix was prepared according to manufacturer's protocol and 10 µL was added to each well of the 96-well plate. Three biological replicates were used for each condition. Reactions were performed using ViiA™ 7 Real-Time PCR System (Life Technologies) with activation for 2 min at 95 °C, followed by 40 cycles of 1s at 95 °C and 20s at 60 °C. Results were calculated using the $2^{-\Delta\Delta Ct}$ relative quantification (RQ) method, relative to vehicle control, and normalized to *HPRT1*, *GUSB* and *GAPDH* reference genes. Multiple t-test with Holm-Sidak correction was performed and adjusted for false discovery rate (FDR), with 5% cut-off.

2.10 qPCR for stem cell-like markers, *NANOG* and *OCT4*

To determine phenotypic changes between 3D-cultured (1-week, 3-weeks, 4-week) to 2D-cultured cells, transcript expression of Nanog homeobox pseudogene-1 (*NANOG*; Hs04399610_g1; Applied Biosystems) and octamer-binding transcription factor-4 (*OCT4*; Hs00742896_s1; Applied Biosystems) were determined by qPCR. Human hypoxanthine phosphoribosyltransferase-1 (*HPRT1*;

Hs99999909_m1; Applied Biosystems) was used as reference gene and 10 µL reactions (1 µL cDNA, 0.5 µL *HPRT1*, 0.5 µL *OCT4/NANOG*, 7 µL TaqMan™ Fast Advanced Master Mix) were performed using conditions in section 2.9. Three biological replicates, with three technical replicates were used. Results were calculated using $2^{-\Delta\Delta Ct}$ RQ method, relative to 2D-cultured cells and normalized to *HPRT1* reference gene.

Similar procedure was performed on 4-week 3D-cultured cells that were reseeded as monolayer required for the drug sensitivity assays (five days), to confirm that *NANOG* and *OCT4* expression was maintained and the cells were phenotypically different to 2D-cultured cells.

2.11 Drug sensitivity assay

The half-maximal inhibitory concentration (IC50) in response to chemotherapies (paclitaxel, doxorubicin, 5-fluorouracil) or bacopaside II were measured and compared between 2D-cultured and 4-weeks 3D-cultured cells. Cells were seeded as monolayer at 3.3×10^3 cells per well in a 96-well flat bottom plates and treated with chemotherapies or bacopaside II shown in Table 1. IC50 was determined using IncucyteS3 confluence measurement at day five. To validate IncucyteS3 results, crystal violet assay (CVA) was performed as described previously[21]. Cells were seeded and treated similarly for five days, before being stained with crystal violet (Sigma-Aldrich). Absorbance was measured at 595 nm using FLUOstar Optima microplate reader (BMG Labtech, Ortenberg, Germany) at day five. Results were analysed using extra sum-of-squares F-test (Prism v8.4.3) to compare IC50 (with 95% CI) between 2D-cultured and 3D-cultured cells (n = 6 per condition).

3. Results:

3.1 Caspase-3/-7 was not activated by bacopaside II

To investigate the type of cell death that had occurred, caspase-3/-7 activation was investigated as a hallmark for apoptosis. Relative to vehicle control, results showed no significant differences in caspase-3/-7 counts with each bacopaside II treatment (Figure 3).

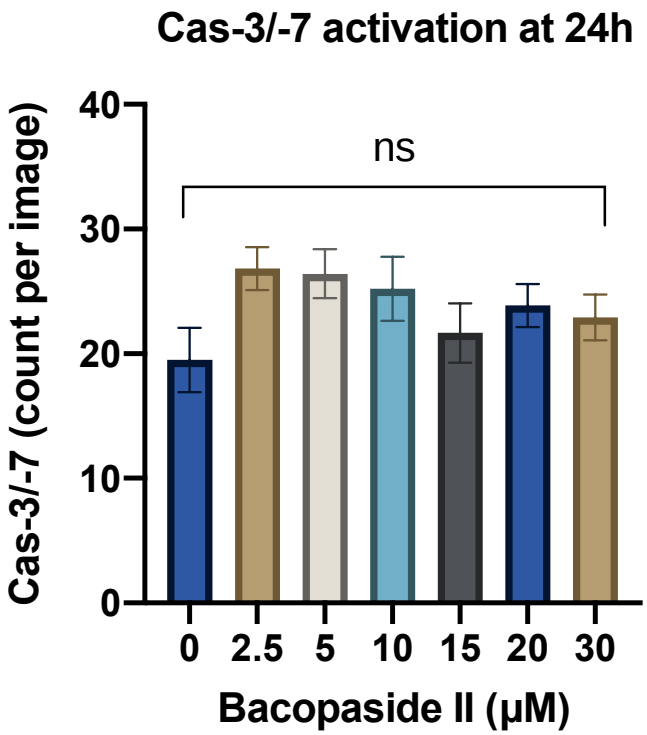

Figure 3: Caspase-3/-7 activation in MDA-MB-231 treated with bacopaside II. Results were analysed using one-way ANOVA with Dunnett's multiple comparison and expressed as mean ± SEM (n = 6). $p > 0.05$ (ns).

3.2 TMR-dextran did not colocalize within vacuoles with bacopaside II treatment

To test whether bacopaside II causes macropinocytosis, TMR-dextran uptake was measured. Vacuole formation was prominent at 6 h of treatment, but 75-kDa TMR-dextran did not colocalize within these vacuoles (Figure 4).

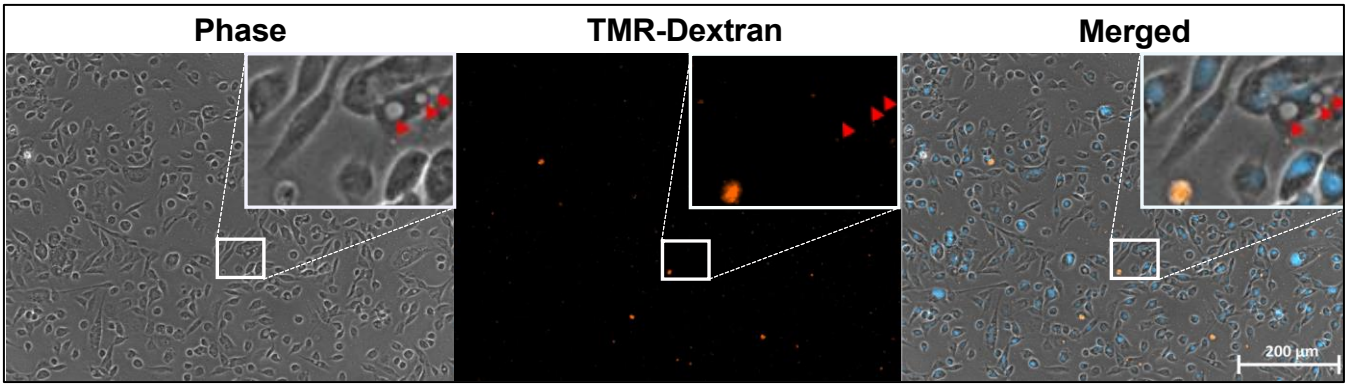

Figure 4: TMR-dextran uptake with bacopaside II. Red arrows: vacuoles; Orange: TMR-dextran; Blue: Nuclei. Representative images (n = 3) were captured at 10X magnification (inset magnified view).

3.3 Membrane integrity was disrupted by bacopaside II

The kinetics of cell membrane permeability with bacopaside II treatment was investigated using PI. PI count increased for each treatment across two days. Comparing to vehicle control, rapid PI-influx was observed with 20 and 30 µM of bacopaside II, whereby significant differences ($p < 0.05$) in PI-influx was observed from time points 4 h and 2 h respectively (Figure 5).

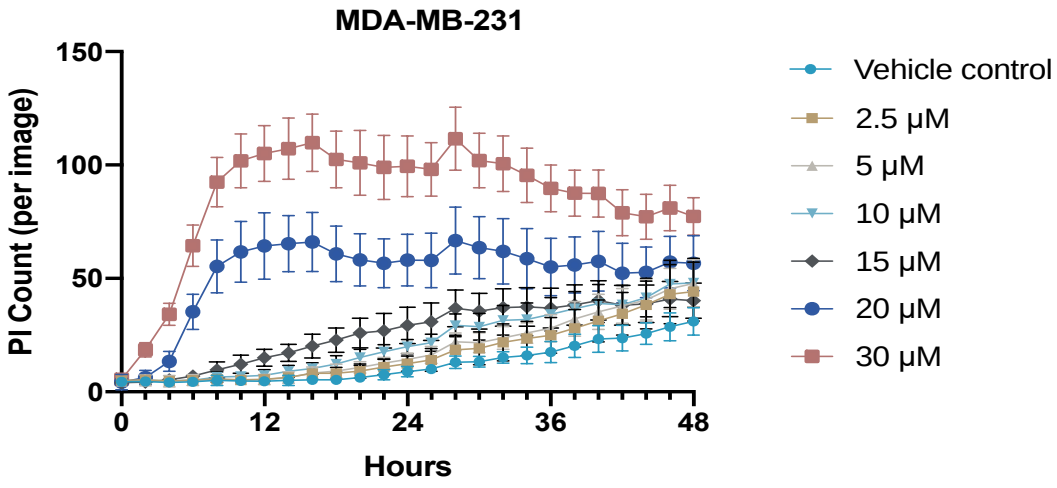

Figure 5: Kinetics of membrane permeability with bacopaside II. Two-way ANOVA with Dunnett's multiple comparison test was used to compare difference in PI-influx relative to vehicle control (n = 6).

3.4 Bacopaside II may induce necroptosis

Since rapid PI-influx was observed with 20 and 30 µM of bacopaside II treatment, the possibility of necroptosis was explored using necrostatin-1, an inhibitor of RIPK1. With 20 µM bacopaside II, 40 and 50 µM necrostatin-1 decreased 20.3% ($p < 0.05$) and 19.8% ($p < 0.05$) of PI count respectively, as compared to vehicle control (Figure 6A). With 30 µM bacopaside II, only 50 µM of necrostatin-1 decreased PI-influx (20.8%, $p < 0.05$) (Figure 6B).

To further validate necroptosis pathway, ratio of the normalized intensity of pMLKL to MLKL (pMLKL:MLKL) protein expression was measured (Figure 6C-6E). With 15, 20 and 30 µM bacopaside II treatment, pMLKL:MLKL increased by 2-fold, 3-fold and 7-fold respectively, relative to vehicle control (Figure 6E). Basal level of pMLKL was also observed in vehicle control (Figure 6D).

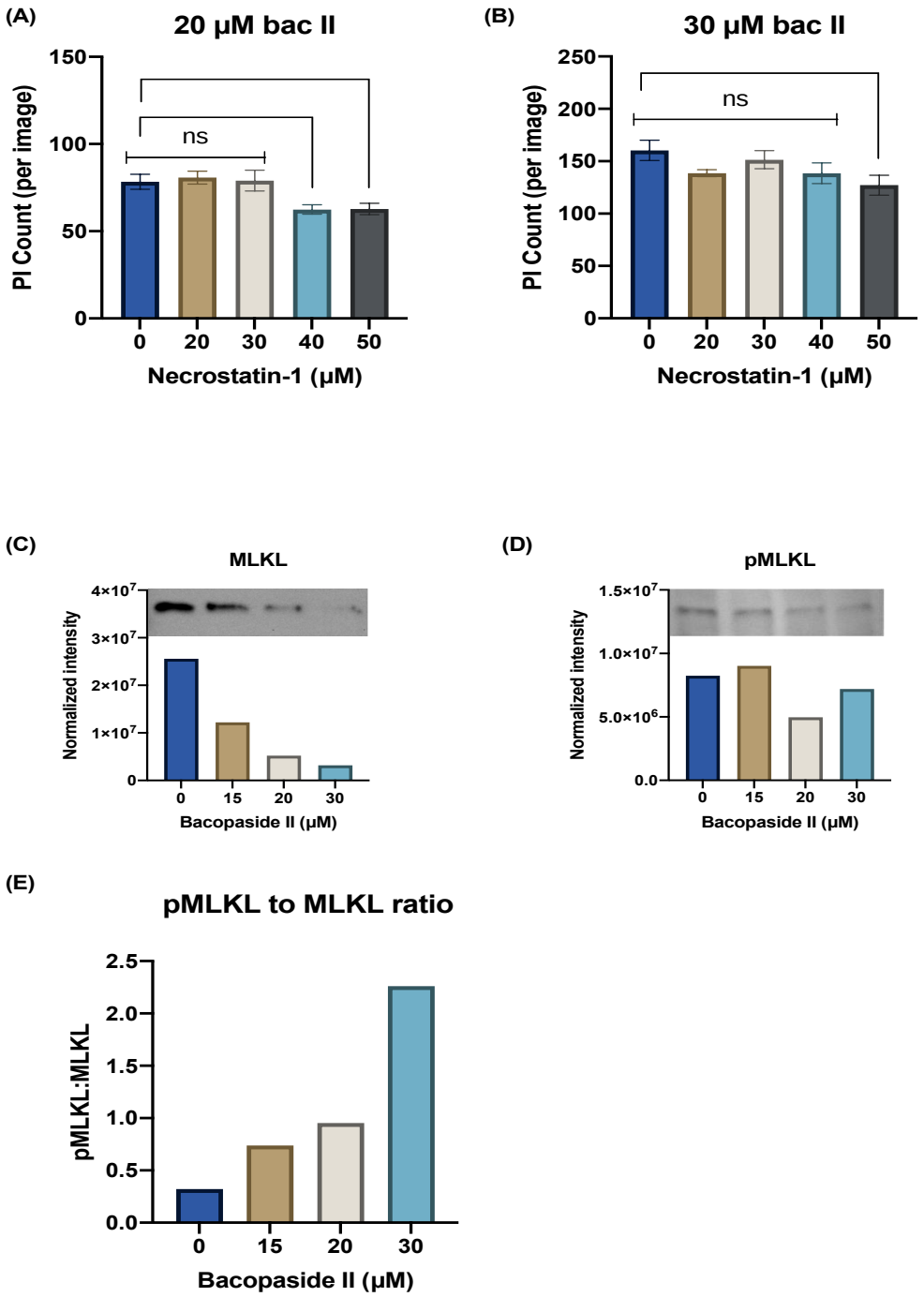

Figure 6: Investigating necroptosis pathway with bacopaside II. PI-influx with various doses of necrostatin-1 and (A) 20 µM or (B) 30 µM bacopaside II treatment at 12h. Results were analysed relative to vehicle control, using one-way ANOVA with Dunnett's multiple comparison and expressed as mean ± SEM (n = 6). * < 0.05, ns > 0.05. Western blot on (C) MLKL, (D) pMLKL and (E) ratio of the normalized intensity of pMLKL to MLKL, with bacopaside II treatment (n = 1).

3.5 Bacopaside II increased *PRKCD* expression

Transcriptomic changes in PI3K-Akt-mTOR signalling pathway with 15 µM bacopaside II treatment was determined using TaqMan® array human PI3K signalling. Relative to vehicle control, only protein kinase C delta transcript (*PRKCD*) displayed significant change, with a 2.2-fold ($p < 0.05$) increase in transcript expression observed (Figure 7).

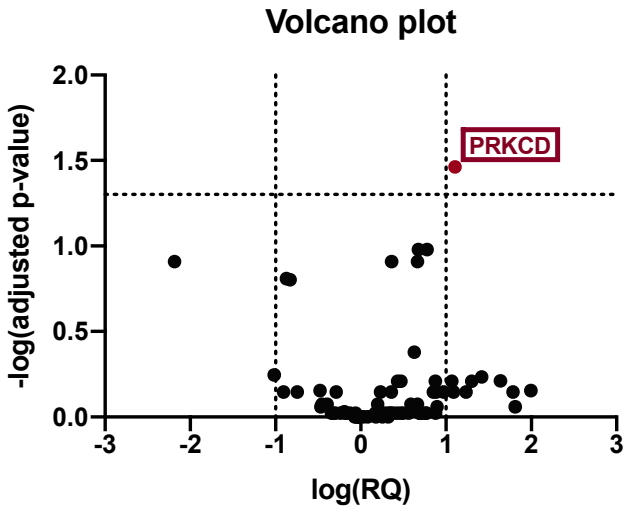

Figure 7: Volcano plot of genes in PI3K-Akt-mTOR signalling pathway. Results were analysed using multiple t-test with Holm-Sidak correction and FDR adjustment (n = 3).

3.6 3D-culture promotes stem cell-like phenotype in MDA-MB-231

To determine if culturing MDA-MB-231 in 3D conditions promoted a stem-cell like phenotype, transcript expression of the stem cell markers, *OCT4* and *NANOG*, were measured and compared between cells grown as a monolayer (2D) to cells grown as 3D mammospheres for 1-, 3- and 4-week (Figure 8). Compared to 2D-cultured cells, *OCT4* increased by 2.4-fold ($p < 0.0001$), 2.6-fold ($p < 0.0001$), and 1.8-fold ($p < 0.001$) after 1-, 3- and 4-week as 3D-cultured cells respectively. Compared to 2D-cultured cells, *NANOG* significantly ($p < 0.0001$) increased by 28-fold, 48-fold and 34-fold after 1-, 3- and 4-weeks as 3D-cultured cells respectively.

To determine if 3D-cultured cells maintained this stem cell-like phenotype after subsequent short-term culture as a monolayer, 4-week 3D-cultured mammospheres were dissociated into single cells and cultured as monolayer for 5 days (3D to 2D). Compared to 2D-cultured cells, *OCT4* and *NANOG* was 3.9-fold ($p < 0.0001$) and 34-fold ($p < 0.0001$) higher respectively, in "3D to 2D" cells. Together, these results demonstrated that culturing MDA-MB-231 cells as 3D mammospheres promoted a stem-cell like phenotype which persisted even after short-term culture as a monolayer.

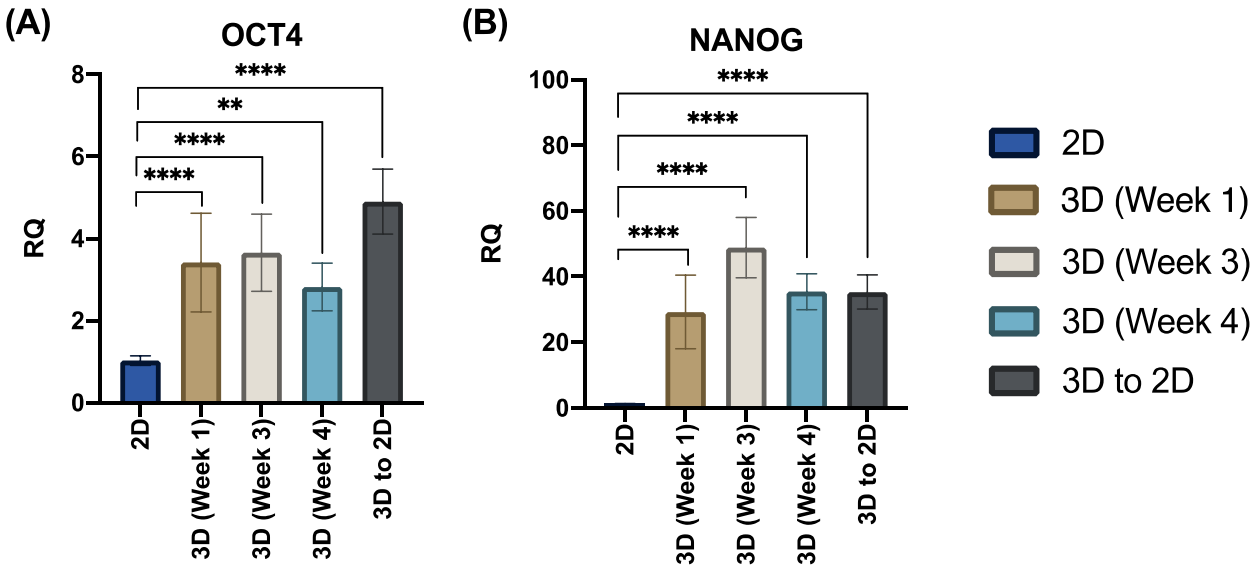

Figure 8: Stem cell-like phenotype in 3D-cultured and 2D-cultured cells. Transcript expression of (A) OCT4 and (B) NANOG of MDA-MB-231 cells in 2D-culture, 3D-culture and cells that were reseeded (3D to 2D) for drug sensitivity assay. Results were analysed using one-way ANOVA test with Dunnett's multiple comparison and RQ with 95% CI were presented. ****$p < 0.0001$, **$p < 0.003$.

3.7 3D-cultured MDA-MB-231 displayed an increase in resistance to paclitaxel, doxorubicin and 5-fluorouracil.

Since there was an increase in stem-like phenotype in the 3D-cultured MDA-MB-231 cells, these cells were further assessed on their response to chemotherapeutics, paclitaxel, doxorubicin and 5-fluorouracil. IC50 for each drug was measured and resistance was indicated by the increase in IC50 in 4-week 3D-cultured cells relative to 2D-cultured cells.

IncucyteS3 confluence data showed an increase in IC50 to paclitaxel (Figure 9A), doxorubicin (Figure 9C) and 5-fluorouracil (Figure 9E) by 2.1-fold ($p < 0.0001$), 2.2-fold ($p < 0.0001$) and 1.4-fold ($p < 0.0001$) respectively, when comparing 3D-cultured cells to 2D-cultured cells.

Crystal violet assay demonstrated a similar increase in IC50 to paclitaxel (Figure 9B), doxorubicin (Figure 9D) and 5-fluorouracil (Figure 9F) of 2.1-fold ($p < 0.0001$), 3.5-fold ($p < 0.0001$) and 1.6-fold ($p < 0.0001$) respectively, when comparing 3D-cultured to 2D-cultured cells.

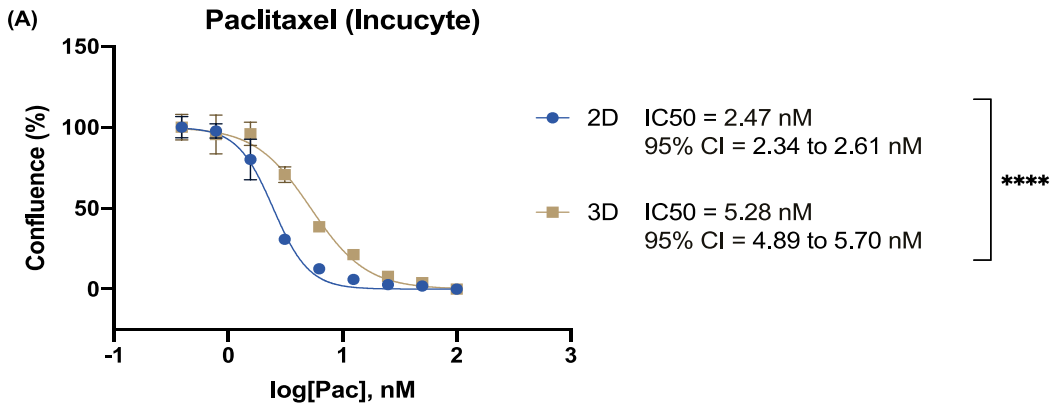
(A)
Paclitaxel (Incucyte)
Confluence (%)
150
100
50
0
-1
0
1
2
3
log[Pac], nM
2D
IC50 = 2.47 nM
95% CI = 2.34 to 2.61 nM
3D
IC50 = 5.28 nM
95% CI = 4.89 to 5.70 nM
****

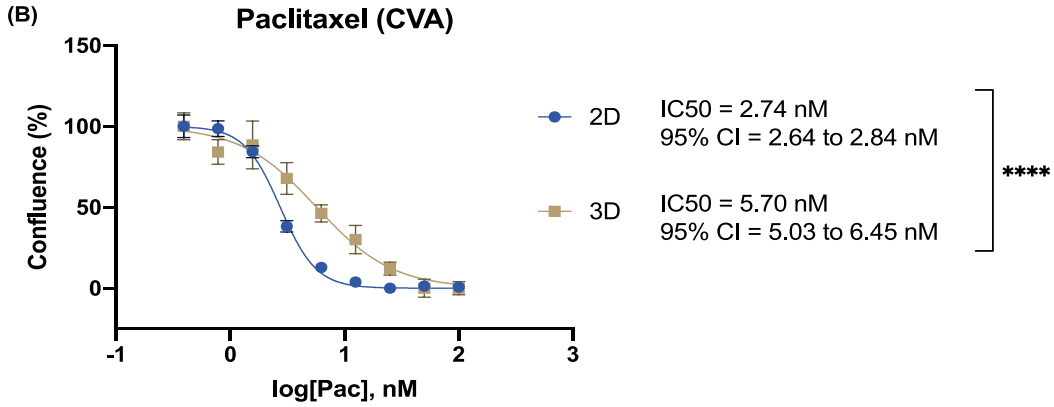
(B)
Paclitaxel (CVA)
Confluence (%)
150
100
50
0
-1
0
1
2
3
log[Pac], nM
2D
IC50 = 2.74 nM
95% CI = 2.64 to 2.84 nM
3D
IC50 = 5.70 nM
95% CI = 5.03 to 6.45 nM
****

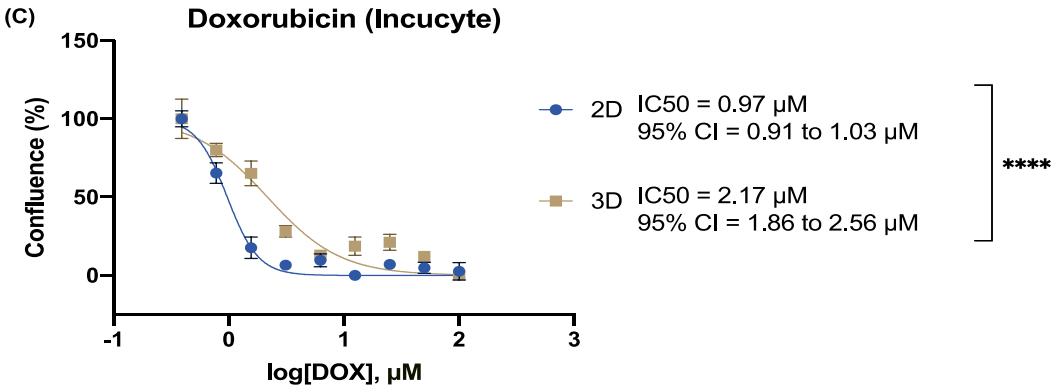
(C)
Doxorubicin (Incucyte)
Confluence (%)
150
100
50
0
-1
0
1
2
3
log[DOX], µM
2D
IC50 = 0.97 µM
95% CI = 0.91 to 1.03 µM
3D
IC50 = 2.17 µM
95% CI = 1.86 to 2.56 µM
****

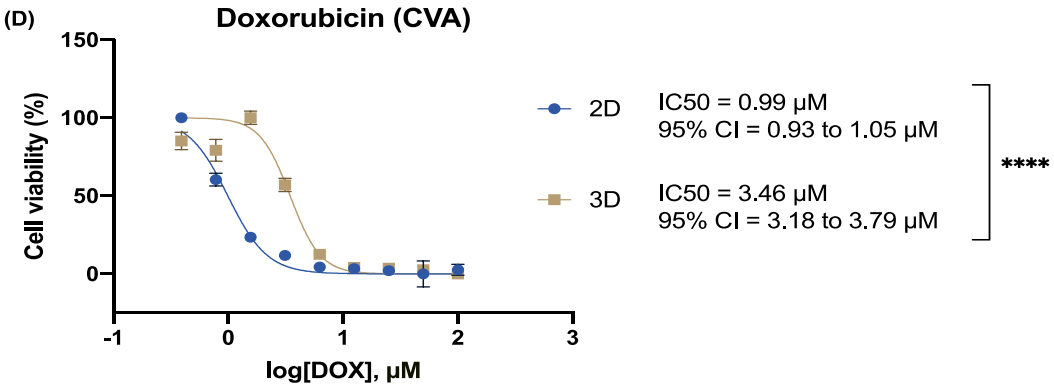
(D)
Doxorubicin (CVA)
Cell viability (%)
150
100
50
0
-1
0
1
2
3
log[DOX], µM
2D
IC50 = 0.99 µM
95% CI = 0.93 to 1.05 µM
3D
IC50 = 3.46 µM
95% CI = 3.18 to 3.79 µM
****

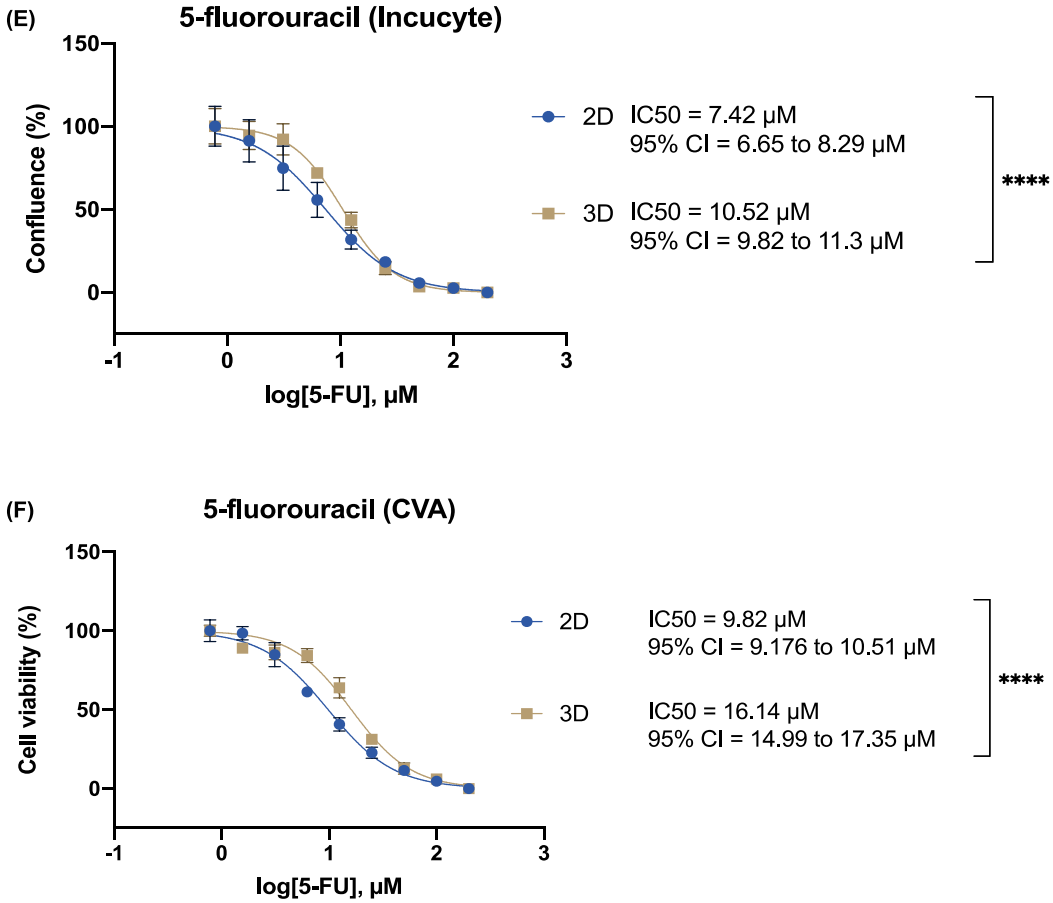

Figure 9: Dose-response curves of chemotherapeutics on 2D-cultured and 3D-cultured MDA-MB-231. IncucyteS3 and CVA data for (A, B) paclitaxel, (C, D) doxorubicin and (E, F) 5-fluorouracil. IC50 with 95% CI were compared between 2D-cultured and 3D-cultured cells using extra sum-of-squares F-test (n = 6). ****p < 0.0001.

3.8 Efficacy of bacopaside II was not altered in 3D-cultured cells

The efficacy of bacopaside II was tested on 3D-cultured cell model. No significant difference (p = 0.71) was observed between the IC50 of bacopaside II in 3D-cultured and 2D-cultured cells, using IncucyteS3 (Figure 10A). Similarly, crystal violet assay showed no significant differences (p = 0.45) between IC50 of bacopaside II in 3D-cultured and 2D-cultured cells (Figure 10B), confirming IncucyteS3 results.

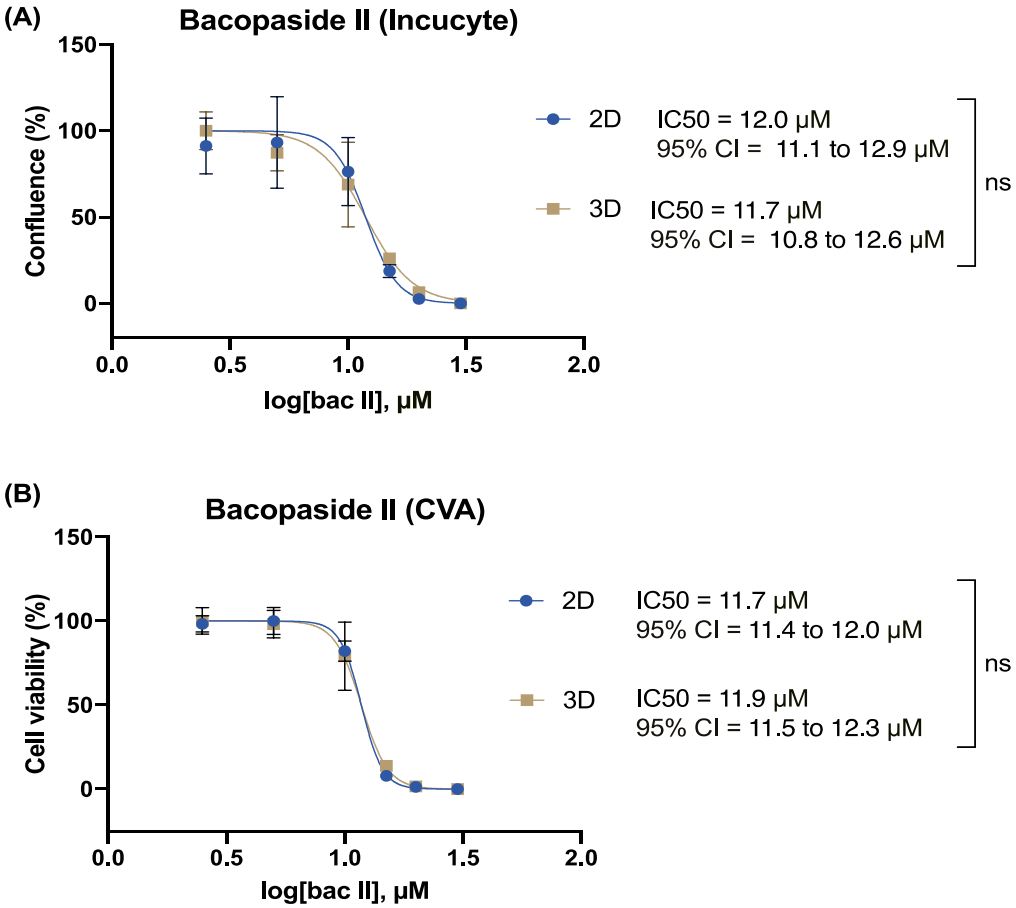

Figure 10: Dose-response curves of bacopaside II on 2D-cultured and 3D-cultured MDA-MB-231. (A) IncucyteS3 and (B) CVA data for bacopaside II dose-response curve. IC50 with 95% CI were compared between 2D-cultured and 3D-cultured cells using extra sum-of-squares F-test (n = 6). ****p < 0.0001, ns – (A) p = 0.71, (B) p = 0.45.

4. Discussion

Bacopaside II has been reported to have anti-tumour effects such as inhibiting cell growth, migration, proliferation and promoting cell death, suggesting its potential as a novel cancer therapeutic[20, 21]. However, the mechanism of cell death of bacopaside II remains unknown. This study is the first to investigate the specific mechanism of cell death with bacopaside II treatment, while exploring transcriptomic changes in the PI3K-Akt-mTOR signalling pathway (Figure 11). Furthermore, drug resistance often develops in TNBC patients[7]. Hence, a resistant TNBC cell model was established to explore the potential of bacopaside II to overcome resistance.

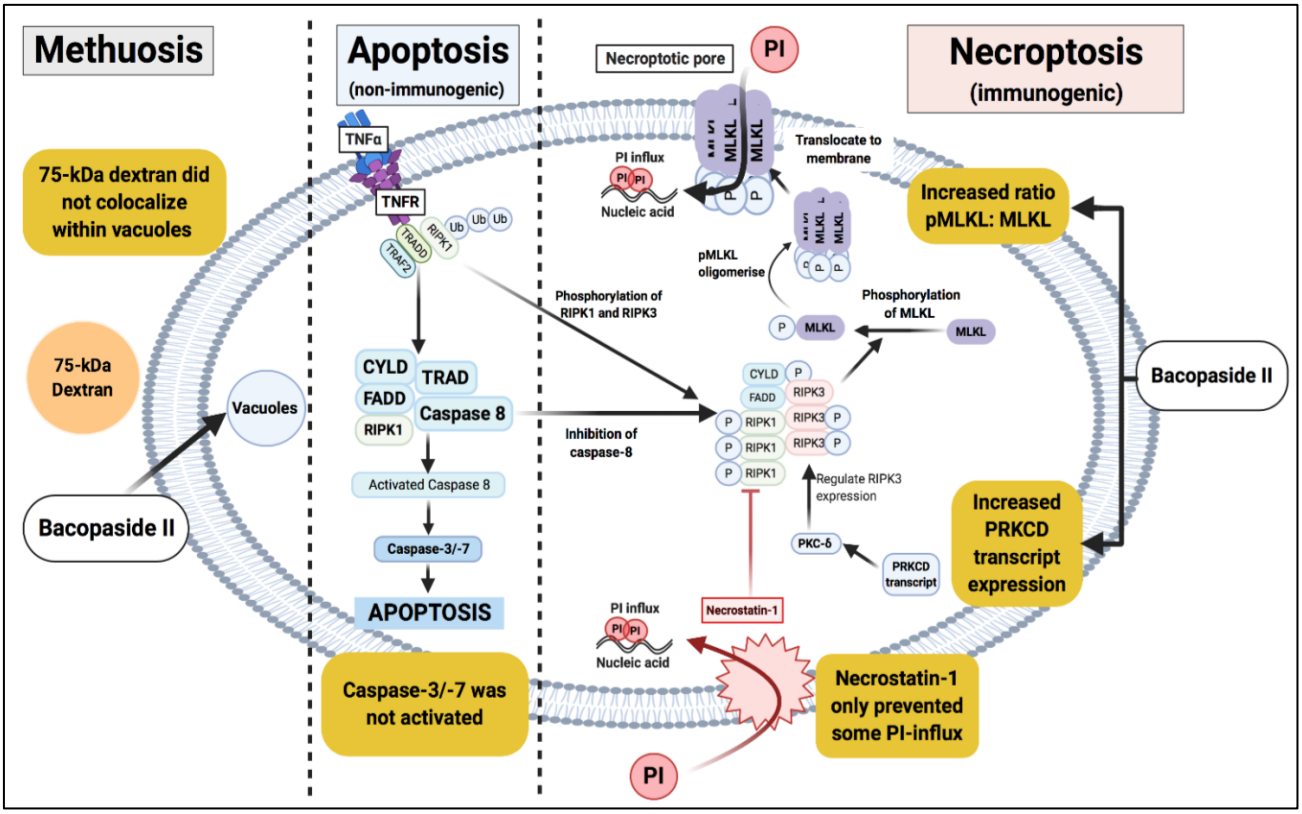

Figure 11: Overview of findings related to methuosis, apoptosis and necroptosis.

Previously, our group suggested that apoptosis had occurred in MDA-MB-231 cells treated with bacopaside II, due to an increase in annexin-V and PI positivity[20]. This study showed that bacopaside II did not induce a significant increase in caspase-3/-7 activation, suggesting that cell death was not apoptosis.

Another prominent event that occurred with bacopaside II treatment was the formation of vacuoles, similar to methuosis[20-22]. During methuosis, excessive macropinocytosis will result in colocalization of macromolecules, such as TMR-dextran, into vacuoles within the cell[24, 25]. In this study, 75-kDa dextran did not colocalize within the vacuoles, suggesting that macropinocytosis did not occur. Methuosis has also been measured using macropinosome markers, in combination with the uptake of different sized molecules such as lucifer yellow (457-Da) or TMR-dextran (10- to 75-kDa)[23-25, 42]. Therefore, the occurrence of methuosis with bacopaside II treatment remains inconclusive.

Subsequently, necroptosis was investigated as a possible mechanism of cell death caused by bacopaside II. In this study, higher doses of bacopaside II (≥ 20 µM) caused rapid PI-influx into the cell, indicating loss of cell membrane integrity and cell death. Necrostatin-1, an inhibitor of necroptosis by upstream inhibition of RIPK1, significantly reduced PI-influx. These findings were the first evidence suggesting that bacopaside II may induce necroptosis. However, necrostatin-1 was unable to block greater amount of PI-influx, indicating the possibility of other cell death mechanisms occurring concurrently such as necrosis.

To provide further evidence that necroptosis occurred, we measured expression of pMLKL and MLKL. We observed basal levels of pMLKL in MDA-MB-231 cells with intact plasma membranes, consistent to findings from Liu *et al.*[43]. Bacopaside II also increased pMLKL:MLKL in a dose-dependent manner, corresponding with PI-uptake. These findings suggest that the ratio of pMLKL to MLKL may be a critical determinant of necroptotic pore formation. Similarly, others have found well-established necroptosis induction method increased pMLKL:MLKL, which coincided with increased lactate dehydrogenase release, annexin-V binding and PI-uptake[44]. Together, this suggests that bacopaside II may induce necroptosis.

To understand the underlying transcriptomic changes with bacopaside II, the PI3K-Akt-mTOR signalling pathway was screened. Significant upregulation of *PRKCD* transcript was observed with

bacopaside II treatment. *PRKCD* encodes for protein kinase C delta (PKC-δ), which belongs to the family of serine and threonine kinase. PKC-δ exhibits both proapoptotic and pro-survival roles in breast cancer and its expression is associated with poorer prognosis in breast cancer patients[45, 46]. PKC-δ was found to regulate expression of key necroptosis protein, RIPK3, resulting in increased necroptotic cell death in smooth muscle cells[47]. Similarly, the elevated expression of *PRKCD* coincided with increased cell death and pMLKL:MLKL in this study, suggesting a possible relationship between bacopaside II, PKC-δ and necroptosis.

Lastly, an MDA-MB-231 resistant model associated with increased stem cell-like phenotype was established through scaffold-less 3D-culture for four weeks. A previous study by Yousefnia S *et al.*[41] reported that doxorubicin resistance in scaffold-less 3D-cultured MDA-MB-231 was associated with an increase in NANOG and OCT4. Other studies have shown 3D-cultures in hydrogel or matrigel scaffolds promotes a stem-cell phenotype and resistance to paclitaxel and doxorubicin in MDA-MB-231[48, 49]. In this study, we showed an increase in resistance towards paclitaxel, doxorubicin and 5-fluorouracil, indicated by increased IC50 in MDA-MB-231 cells grown in scaffold-less 3D-culture, as compared to 2D-cultured cells. Resistance in breast CSC can be associated with increased drug efflux pumps (ABCG2; breast cancer resistance protein) and overactivation of anti-apoptotic signalings (PI3K-Akt-mTOR pathway)[50]. Unlike other chemotherapeutics in this study, similar IC50 was found in 2D-cultured and 3D-cultured cells, indicating no increase in resistance towards bacopaside II. This shows that this chemotherapy drug resistant model retained sensitivity to bacopaside II, suggesting that bacopaside II may have the potential to overcome chemo-resistance in cancer patients.

4.1 Limitations and future directions

This study focused only on TNBC mesenchymal cell line, MDA-MB-231, and may not be representative of other TNBC subtypes. Future studies can include other cell types, including normal

cells, to capture a wider perspective of the effects of bacopaside II. This study also lacked positive controls such as TSI (TNF, Smac mimetic, IDN-6556) and vacuolin-1 for necroptosis and methuosis respectively, which will provide greater certainty to current findings[24, 44]. Future studies should also include key vacuole markers (Rab-7 and LAMP1) and necroptosis proteins (RIPK1, RIPK3) as validation for methuosis and necroptosis respectively[24, 44].

Since necroptosis is an immunogenic cell death which releases DAMPs, chemokines, cytokines, and recruits cytotoxic T-cells, it has clinical importance as an adjunct to immunotherapy. Patients previously unresponsive to immunotherapy may be sensitised following bacopaside II treatment. Future *in vivo* studies will be essential to evaluate the immune response in combination with checkpoint inhibition.

5. Conclusion

In summary, this study highlights necroptosis as a possible mechanism of cell death of bacopaside II in TNBC. Furthermore, efficacy of bacopaside II was not affected in the established resistant model. Further studies will be required to validate the mechanism of cell death and determine the potential of bacopaside II as a therapeutic agent for TNBC, alone or in combination with immunotherapy.

Professional and funding acknowledgements

This study acknowledges the funding support from Margaret Elcombe Grant, The Hospital Research Foundation and The Hospital Foundation Honours Scholarship.

I would like to thank my supervisors, Dr Jennifer Hardingham and Dr Eric Smith, for providing me the opportunity for an honours project, assisting in the application for the Hospital Foundation scholarship, teaching and providing technical assistance when needed, while also providing constructive criticisms and challenging my thoughts throughout the year.

References

1. Bray F, Ferlay J, Soerjomataram I, Siegel RL, Torre LA & Jemal A (2018). Global cancer statistics 2018: GLOBOCAN estimates of incidence and mortality worldwide for 36 cancers in 185 countries. *CA Cancer J Clin.* **68**, 394-424.

2. Garrido-Castro AC, Lin NU & Polyak K (2019). Insights into Molecular Classifications of Triple-Negative Breast Cancer: Improving Patient Selection for Treatment. *Cancer Discov.* **9**, 176-198.

3. O'Reilly EA, Gubbins L, Sharma S, Tully R, Guang MHZ, Weiner-Gorzel K, McCaffrey J, Harrison M, Furlong F, Kell M & McCann A (2015). The fate of chemoresistance in triple negative breast cancer (TNBC). *BBA Clinical.* **3**, 257-275.

4. Al-Mahayri ZN, Patrinos GP & Ali BR (2020). Toxicity and Pharmacogenomic Biomarkers in Breast Cancer Chemotherapy. *Front. Pharmacol.* **11**, 445.

5. Jézéquel P, Kerdraon O, Hondermarck H, Guérin-Charbonnel C, Lasla H, Gouraud W, Canon J-L, Gombos A, Dalenc F, Delaloge S, Lemonnier J, Loussouarn D, Verrièle V & Campone M (2019). Identification of three subtypes of triple-negative breast cancer with potential therapeutic implications. *Breast Cancer Res.* **21**, 65.

6. Butti R, Gunasekaran VP, Kumar TVS, Banerjee P & Kundu GC (2019). Breast cancer stem cells: Biology and therapeutic implications. *Int. J. Biochem. Cell. Biol.* **107**, 38-52.

7. Bianchini G, Balko JM, Mayer IA, Sanders ME & Gianni L (2016). Triple-negative breast cancer: challenges and opportunities of a heterogeneous disease. *Nat. Rev. Clin. Oncol.* **13**, 674-690.

8. Lee KL, Kuo YC, Ho YS & Huang YH (2019). Triple-Negative Breast Cancer: Current Understanding and Future Therapeutic Breakthrough Targeting Cancer Stemness. *Cancers.* **11**, 1334.

9. Nagata T, Shimada Y, Sekine S, Moriyama M, Hashimoto I, Matsui K, Okumura T, Hori T, Imura J & Tsukada K (2017). KLF4 and NANOG are prognostic biomarkers for triple-negative breast cancer. *Breast Cancer.* **24**, 326-335.

10. Zhang J-M, Wei K & Jiang M (2018). OCT4 but not SOX2 expression correlates with worse prognosis in surgical patients with triple-negative breast cancer. *Breast Cancer.* **25**, 447-455.

11. Aguiar S & Borowski T (2013). Neuropharmacological Review of the Nootropic Herb Bacopa monnieri. *Rejuvenation Res.* **16**, 313-326.

12. Peng L, Zhou Y, Kong de Y & Zhang WD (2010). Antitumor activities of dammarane triterpene saponins from Bacopa monniera. *Phytother. Res.* **24**, 864-8.

13. Russo A & Borrelli F (2005). Bacopa monniera, a reputed nootropic plant: an overview. *Phytomedicine.* **12**, 305-317.

14. Du JR, Long FY & Chen C (2014). Research Progress on Natural Triterpenoid Saponins in the Chemoprevention and Chemotherapy of Cancer. In *Natural Products and Cancer Signaling: Isoprenoids, Polyphenols and Flavonoids*, 1st edn, ed. Bathaie SZ & Tamanoi F, 95-130. Academic Press, Cambridge, Massachusetts, United States.

15. Mallick MN, Akhtar MS, Najm MZ, Tamboli ET, Ahmad S & Husain SA (2015). Evaluation of anticancer potential of Bacopa monnieri L. against MCF-7 and MDA-MB 231 cell line. *J. Pharm. Bioallied. Sci.* **7**, 325-328.

16. Mallick MN, Khan W, Parveen R, Ahmad S, S, Najm M, Ahmad I & Husain S (2017). Exploring the cytotoxic potential of triterpenoids-enriched fraction of Bacopa monnieri by implementing In vitro, In vivo, and In silico approaches. *Pharmacogn. Mag.* **13**, 595-606.

17. John S, Sivakumar KC & Mishra R (2017). Bacoside A Induces Tumor Cell Death in Human Glioblastoma Cell Lines through Catastrophic Macropinocytosis. *Front. Mol. Neurosci.* **10**, 171.

18. Aithal MGS & Rajeswari N (2019). Bacoside A Induced Sub-G0 Arrest and Early Apoptosis in Human Glioblastoma Cell Line U-87 MG through Notch Signaling Pathway. *Brain Tumor Res. Treat.* **7**, 25-32.

19. Pei JV, Kourghi M, De Ieso ML, Campbell EM, Dorward HS, Hardingham JE & Yool AJ (2016). Differential Inhibition of Water and Ion Channel Activities of Mammalian Aquaporin-1 by Two Structurally Related Bacopaside Compounds Derived from the Medicinal Plant Bacopa monnieri. *Mol. Pharmacol.* **90**, 496-507.

20. Palethorpe HM, Smith E, Tomita Y, Nakhjavani M, Yool AJ, Price TJ, Young JP, Townsend AR & Hardingham JE (2019). Bacopasides I and II Act in Synergy to Inhibit the Growth, Migration and Invasion of Breast Cancer Cell Lines. *Molecules.* **24**, 3539.

21. Smith E, Palethorpe HM, Tomita Y, Pei JV, Townsend AR, Price TJ, Young JP, Yool AJ & Hardingham JE (2018). The Purified Extract from the Medicinal Plant Bacopa monnieri, Bacopaside II, Inhibits Growth of Colon Cancer Cells In Vitro by Inducing Cell Cycle Arrest and Apoptosis. *Cells.* **7**, 81.

22. Palethorpe HM, Tomita Y, Smith E, Pei JV, Townsend AR, Price TJ, Young JP, Yool AJ & Hardingham JE (2018). The aquaporin 1 inhibitor bacopaside II reduces endothelial cell migration and tubulogenesis and induces apoptosis. *Int. J. Mol. Sci.* **19**, 653.

23. Huang W, Sun X, Li Y, He Z, Li L, Deng Z, Huang X, Han S, Zhang T, Zhong J, Wang Z, Xu Q, Zhang J & Deng X (2018). Discovery and Identification of Small Molecules as Methuosis Inducers with in Vivo Antitumor Activities. *J. Med. Chem.* **61**, 5424-5434.

24. Maltese WA & Overmeyer JH (2014). Methuosis: Nonapoptotic Cell Death Associated with Vacuolization of Macropinosome and Endosome Compartments. *Am. J. Pathol.* **184**, 1630-1642.

25. Maltese WA & Overmeyer JH (2015). Non-apoptotic cell death associated with perturbations of macropinocytosis. *Front. Physiol.* **6**, 38.

26. Niu G & Chen X (2010). Apoptosis Imaging: Beyond Annexin V. *J. Nucl. Med.* **51**, 1659-1662.

27. Pietkiewicz S, Schmidt JH & Lavrik IN (2015). Quantification of apoptosis and necroptosis at the single cell level by a combination of Imaging Flow Cytometry with classical Annexin V/propidium iodide staining. *J. Immunol. Methods.* **423**, 99-103.

28. Zargarian S, Shlomovitz I, Erlich Z, Hourizadeh A, Ofir-Birin Y, Croker BA, Regev-Rudzki N, Edry-Botzer L & Gerlic M (2017). Phosphatidylserine externalization, "necroptotic bodies" release, and phagocytosis during necroptosis. *PLoS Biol.* **15**, e2002711.

29. Kaczmarek A, Vandenabeele P & Krysko Dmitri V (2013). Necroptosis: The Release of Damage-Associated Molecular Patterns and Its Physiological Relevance. *Immunity.* **38**, 209-223.

30. Grootjans S, Vanden Berghe T & Vandenabeele P (2017). Initiation and execution mechanisms of necroptosis: an overview. *Cell Death Differ.* **24**, 1184-1195.

31. Chen X, Li W, Ren J, Huang D, He WT, Song Y, Yang C, Li W, Zheng X, Chen P & Han J (2014). Translocation of mixed lineage kinase domain-like protein to plasma membrane leads to necrotic cell death. *Cell Res.* **24**, 105-21.

32. Cai Z, Jitkaew S, Zhao J, Chiang H-C, Choksi S, Liu J, Ward Y, Wu L-g & Liu Z-G (2014). Plasma membrane translocation of trimerized MLKL protein is required for TNF-induced necroptosis. *Nat. Cell. Biol.* **16**, 55-65.

33. Xia B, Fang S, Chen X, Hu H, Chen P, Wang H & Gao Z (2016). MLKL forms cation channels. *Cell Res.* **26**, 517-28.

34. Wlodkowic D, Telford W, Skommer J & Darzynkiewicz Z (2011). Apoptosis and beyond: cytometry in studies of programmed cell death. *Methods Cell Biol.* **103**, 55-98.

35. Yang J, Nie J, Ma X, Wei Y, Peng Y & Wei X (2019). Targeting PI3K in cancer: mechanisms and advances in clinical trials. *Mol. Cancer.* **18**, 26.

36. Xu F, Na L, Li Y & Chen L (2020). Roles of the PI3K/AKT/mTOR signalling pathways in neurodegenerative diseases and tumours. *Cell Biosci.* **10**, 54.

37. Srivastava RK, Li C, Khan J, Banerjee NS, Chow LT & Athar M (2019). Combined mTORC1/mTORC2 inhibition blocks growth and induces catastrophic macropinocytosis in cancer cells. *Proc. Natl. Acad. Sci. U.S.A.* **116**, 24583.

38. Hu S, Chang X, Zhu H, Wang D & Chen G (2020). PI3K mediates tumor necrosis factor induced-necroptosis through initiating RIP1-RIP3-MLKL signaling pathway activation. *Cytokine.* **129**, 155046.

39. Mohammad RM, Muqbil I, Lowe L, Yedjou C, Hsu H-Y, Lin L-T, Siegelin MD, Fimognari C, Kumar NB, Dou QP, Yang H, Samadi AK, Russo GL, Spagnuolo C, Ray SK,

Chakrabarti M, Morre JD, Coley HM, Honoki K, Fujii H, Georgakilas AG, Amedei A, Niccolai E, Amin A, Ashraf SS, Helferich WG, Yang X, Boosani CS, Guha G, Bhakta D, Ciriolo MR, Aquilano K, Chen S, Mohammed SI, Keith WN, Bilsland A, Halicka D, Nowsheen S & Azmi AS (2015). Broad targeting of resistance to apoptosis in cancer. *Semin. Cancer Biol.* **35**, S78-S103.

40. Mishra R & Bhowmick NA (2019). Visualization of Macropinocytosis in Prostate Fibroblasts. *Bio. Protoc.* **9**, e3235.

41. Yousefnia S, Ghaedi K, Seyed Forootan F & Nasr Esfahani MH (2019). Characterization of the stemness potency of mammospheres isolated from the breast cancer cell lines. *Tumour Biol.* DOI:10.1177/1010428319869101.

42. Li L, Wan T, Wan M, Liu B, Cheng R & Zhang R (2015). The effect of the size of fluorescent dextran on its endocytic pathway. *Cell Biol. Int.* **39**, 531-539.

43. Liu X, Zhou M, Mei L, Ruan J, Hu Q, Peng J, Su H, Liao H, Liu S, Liu W, Wang H, Huang Q, Li F & Li CY (2016). Key roles of necroptotic factors in promoting tumor growth. *Oncotarget.* **7**, 22219-22233.

44. Samson AL, Zhang Y, Geoghegan ND, Gavin XJ, Davies KA, Mlodzianoski MJ, Whitehead LW, Frank D, Garnish SE, Fitzgibbon C, Hempel A, Young SN, Jacobsen AV, Cawthorne W, Petrie EJ, Faux MC, Shield-Artin K, Lalaoui N, Hildebrand JM, Silke J, Rogers KL, Lessene G, Hawkins ED & Murphy JM (2020). MLKL trafficking and accumulation at the plasma membrane control the kinetics and threshold for necroptosis. *Nat. Commun.* **11**, 3151.

45. Allen-Petersen BL, Carter CJ, Ohm AM & Reyland ME (2014). Protein kinase Cδ is required for ErbB2-driven mammary gland tumorigenesis and negatively correlates with prognosis in human breast cancer. *Oncogene.* **33**, 1306-1315.

46. Kang J-H (2014). Protein Kinase C (PKC) Isozymes and Cancer. *New J. Sci.* **2014**, 36.

47. Wang Q, Liu Z, Ren J, Morgan S, Assa C & Liu B (2015). Receptor-interacting protein kinase 3 contributes to abdominal aortic aneurysms via smooth muscle cell necrosis and inflammation. *Circ. Res.* **116**, 600-11.

48. Huang Z, Yu P & Tang J (2020). Characterization of Triple-Negative Breast Cancer MDA-MB-231 Cell Spheroid Model. *OncoTargets Ther.* **13**, 5395-5405.

49. Reynolds DS, Tevis KM, Blessing WA, Colson YL, Zaman MH & Grinstaff MW (2017). Breast Cancer Spheroids Reveal a Differential Cancer Stem Cell Response to Chemotherapeutic Treatment. *Sci. Rep.* **7**, 10382.

50. Bai X, Ni J, Beretov J, Graham P & Li Y (2018). Cancer stem cell in breast cancer therapeutic resistance. *Cancer Treat. Rev.* **69**, 152-163.